Supplementary Material for:

Active touch sensing in the rat: Anticipatory and regulatory control of whisker movements during surface exploration

Robyn A. Grant, Ben Mitchinson, Charles W. Fox, and Tony J. Prescott
Department of Psychology, University of Sheffield, UK

1 Recording apparatus and overhead tracking methods

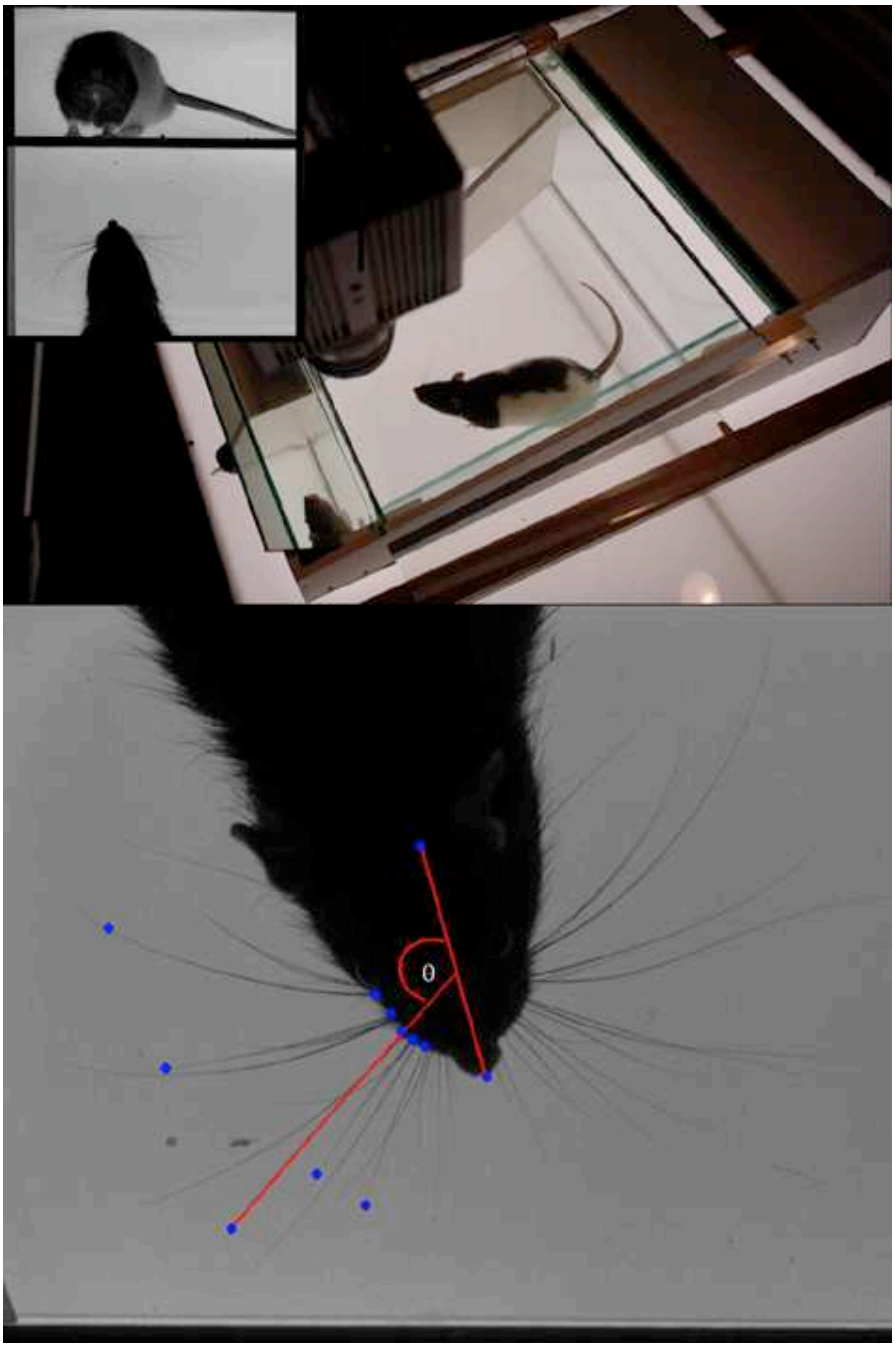

Figure S1. Recording and tracking methods. *Top:* The high-speed camera was positioned above a purpose-built viewing arena illuminated by a light-box. 3-4s recordings are captured opportunistically, and in two viewing planes (horizontal and vertical) whenever the animal enters a 20x20x8 cm viewing area. The inset shows the camera view. *Bottom:* Screen-shot showing tracked points (blue) and oriented lines (red) indicating how whisker angular positions were estimated in each frame.

2 3D Whisker tip tracking methodolology

Arena calibration
At the beginning of each filming session the camera was positioned on the z-axis (approximately 500millimetres above the floor plane), and the mirror aligned manually, so that the top-down and side-on view (via the mirror) were looking directly along the z-/y-axis (see Figure 1 in main article). A calibration shot was then taken of a specialized calibration tool, located at a known position in the arena. From the recorded footage, a calibration program allowed the tracker to identify seven localizable points of the tool, which were then used to calibrate the camera model (Tsai, 1987) using linear optimization. All clips belonging to that session would thus be pre-calibrated.

Tracking whisker tips
Whiskers tips were tracked manually in video-clips displayed at pixel-for-pixel, or greater, resolution on a flat-panel LCD screen. To evaluate how accurately the whiskers tips could be located, a γ macrovibrissa was mounted on a slide that was then positioned at a 45° slant in the arena so that it was visible in both camera views. An image of the slide taken from the high speed video camera was compared with a light microscope photograph of the same slide (Figure S1). This comparison suggested that the video was of sufficient quality to allow the larger whiskers to be seen to within 1-3millimetres of the tip when stationary (93-98% of whisker length).

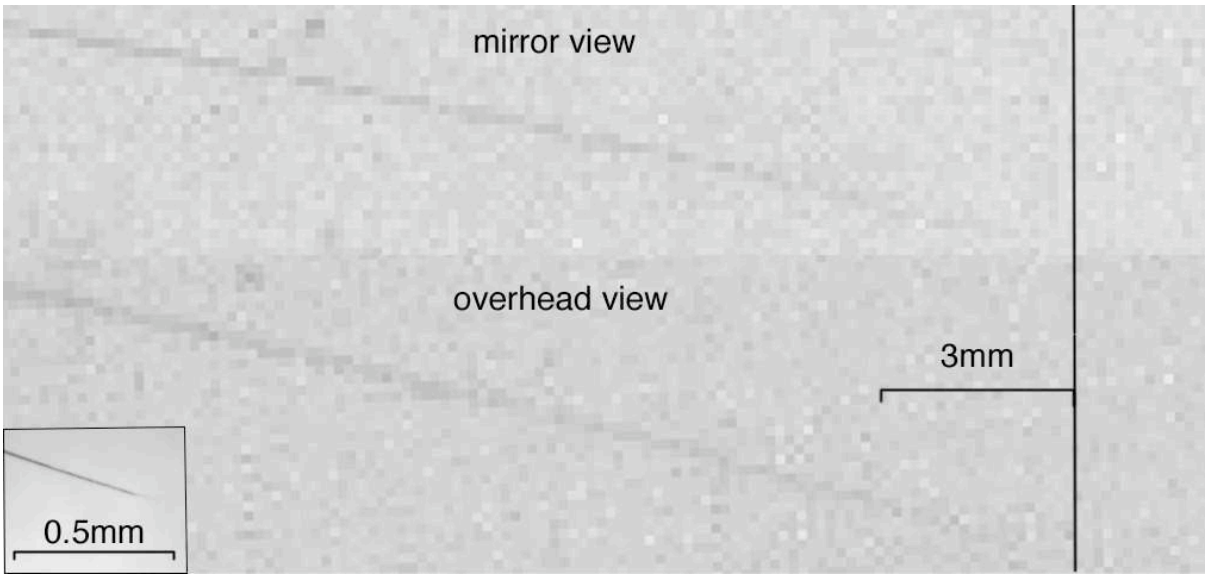

Figure S2. Mirror (side-on) and overhead views of a slide-mounted γ macro-vibrissa as imaged by the HSV camera. The vertical rule shows the position of the whisker tip as estimated from a light microscope photograph of the same whisker (inset). The image indicates that the tips of stationary whiskers can be detected with an accuracy of 1-3 millimetres.

Sections of video were selected in which the majority of whiskers on at least one side of the face were visible in both views throughout the full three whisks. Candidate whisker-tips were labeled for tracking in the first frame of the first whisk cycle and then tracked in each frame for either one (Figure 9) or three (Figure 8) whisk cycles. The raw data generated was a number of image 'tracks' in each view that were each assumed to represent the motion of a unique whisker tip.

Stereo correspondence
It was assumed that at least some of the whisker tips labeled in each view were images of the same whiskers. Identifying pairs of tracks, one from each view that represented the same tips was a matter of assessing 'stereo correspondence'. Each tracked point was transformed into a line in world-space, a 'world-line', by applying the calibrated camera model in reverse. Thus, the tracks which were the raw

data from the observer each generated a 'world-line series', with one world-line for each frame. If two points marked in the two views of a single frame are images of the same object, their world-lines are expected to approach intersection, and the point of intersection is the location of the object in 3D space. Spurious intersections are expected in single frames due to stereo ambiguity, but since the tracked objects are moving over time, these are expected to be transient. Conversely, world-line series that genuinely correspond to the same object will approximately intersect in *all* frames of a clip section. Thus, pairs of tracks that genuinely represent a single object in the world can be identified by consistently low world-line intersection error in all tracked frames (giving the motion of the tracked object over time in 3D space). The matching process used was as follows.

For the two clips illustrated in Figure 8, that were used to calculate a 3D measure of spread, 8 and 10 whisker tips respectively were tracked in each view by a single observer. For each possible pairing of one whisker track from each view (i.e. 64–100 possible pairings) and for each frame, an error metric was computed as the minimum Euclidean distance between the world-lines (that is, world-line intersection error). For the pairing overall, the error was recorded as the root mean square of this error over all trackable frames (using mean square emphasizes large errors in single frames, which should never arise for matched pairs). The pairing with the lowest error was then taken to be a match, the track from each view was eliminated, and the process was repeated until no further pairings remained. With 35 whiskers per side of the face, and 8-10 whiskers tracked in each view, the expected number of matches is 2.9. This is likely to be higher in practice, however, since some whiskers are more prominent than others. We chose to take the top three matches in each of our clips, and confirmed that the errors over time in these cases were in the normal tracking error range. The mean 3D spread was then calculated as the mean Euclidean distances between these best three whisker matches.

For the two clips tracked in Figure 9, 18-19 (left) and 20-14 (right) whisker tips were tracked in both views by three observers. For each whisker-tip, a measure of inter-observer reliability e was then calculated as the average, over all tracked frames, of the distance between the position estimates generated by observers. Whisker-tips for which $e>e(max)$, or that that were marked as untrackable in 1 or more frames by one or more observers were excluded from further analysis; for all remaining whisker-tips estimated trajectories were calculated by averaging across observers. The 3d reconstruction algorithm subsequently made 16 and 13 matches, respectively.

Reference

Tsai, Roger Y. (1987) "A versatile camera calibration technique for high-accuracy 3D machine vision metrology using off-the-shelf TV cameras and lenses,'' *IEEE Journal of Robotics and Automation*, Vol. RA–3, No. 4, August 1987, pp. 323–344.

3 Analysis of spread by contact type

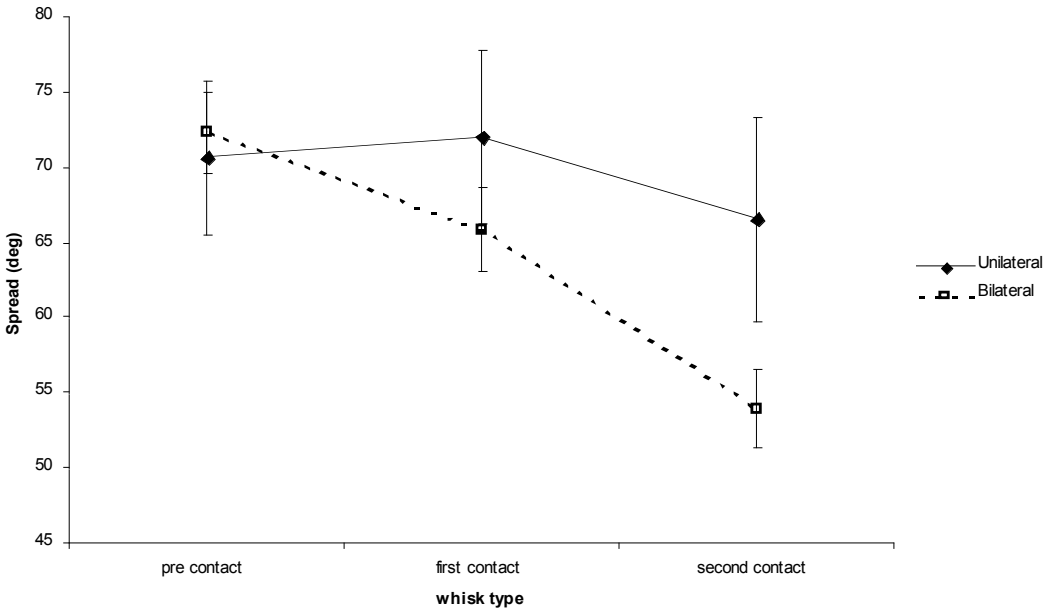

Figure S3. Change in spread across whisk types for unilateral and bilateral first contacts. The graph shows a more pronounced effect on whisker spread in both 1st and 2nd contact whisks when there are bilateral contacts in the 1st contact whisk. Means (s.d.s) for pre-, 1st and 2nd contact whisks were unilateral 70.6 (20.3), 72.0 (23.2), 66.5 (27.4); bilateral 72.3 (17.8), 65.8 (18.4), 53.9 (17.2).

4 Whisker spread and correlated whisker control parameters

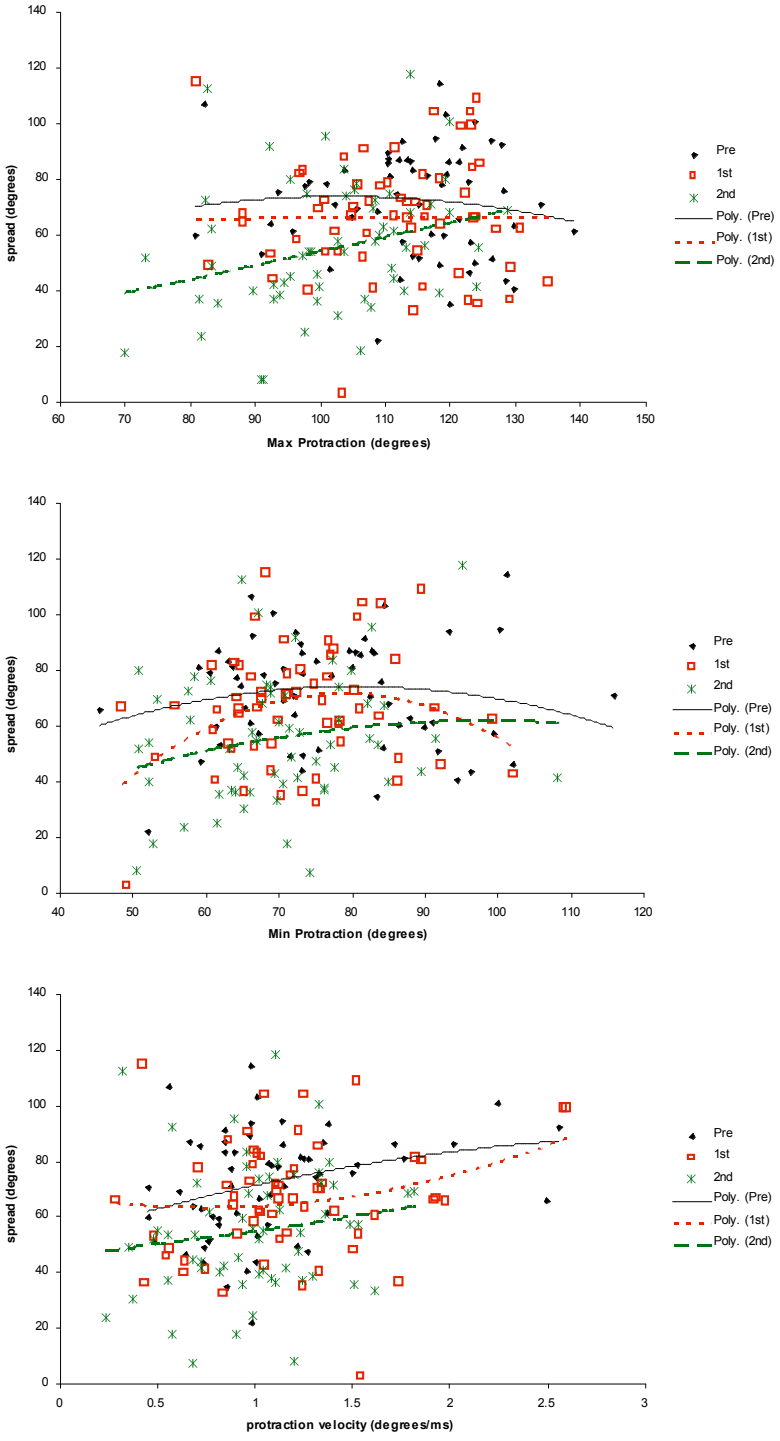

Figure S4. Scatterplots of whisker spread against covarying whisk parameters with polynomial best-fit curves for different whisk types. *Top:* Mean protraction velocity increases with greater whisker spread for all whisk types (Pearson's r= 0.254, p=0.001), however, there is evidence of reduced spread in the 2nd contact whisk across the full range of velocities (that is, the curve for the 2nd contact whisk is below that for the other two whisk types across the full velocity range) which suggests no interaction with whisk type. *Center and Bottom:* For both minimum and maximum protraction there is some convergence of spread values for different whisk types for large values of maximum protraction, and for both large and small values of minimum protraction. Note that Analysis of Covariance (ANCOVA) cannot be used to examine these relationship because of the non-linearities present.

5 Regression analysis for the number of contacts on tracked whiskers

Potential predictors

Geometric, or head/body movement	*Pearson's r*	*p*
Distance to wall	-0.086	0.348
Inverse distance to wall	+0.104*	0.258
Head orientation	-0.107*	0.244
Snout elevation	+0.332*	<0.001
Velocity towards wall	+0.052	0.575
Whisker control		
Mean protraction velocity	-0.185*	0.073
Mean retraction velocity	-0.129*	0.160
Mean spread	-0.279	0.002
Inverse mean spread	+0.336*	<0.001

Correlations calculated for all 1st and 2nd contact whisks (n= 120)
*= selected for inclusion in regression (r>0.1)

Final model for number of contacts
Adjusted R square= 0.136, $F_{(1,118)} = 10.388$, $p<0.001$ (using the step-wise method)

Predictor variable	*β*	*p*	*Part correlation*
Inverse mean spread	0.230	0.019	0.202
Snout elevation	0.222	0.024	0.195

Inverse distance to wall, head orientation, and mean protraction and retraction velocities were not significant predictors.

Comment. The model is a relatively week predictor explaining just 13.6% of the variance. We suspect that this is, at least in part, because of the poor resolution of the number of contacts measure which only includes contacts on tracked whiskers and thus has a range of just 2–5.

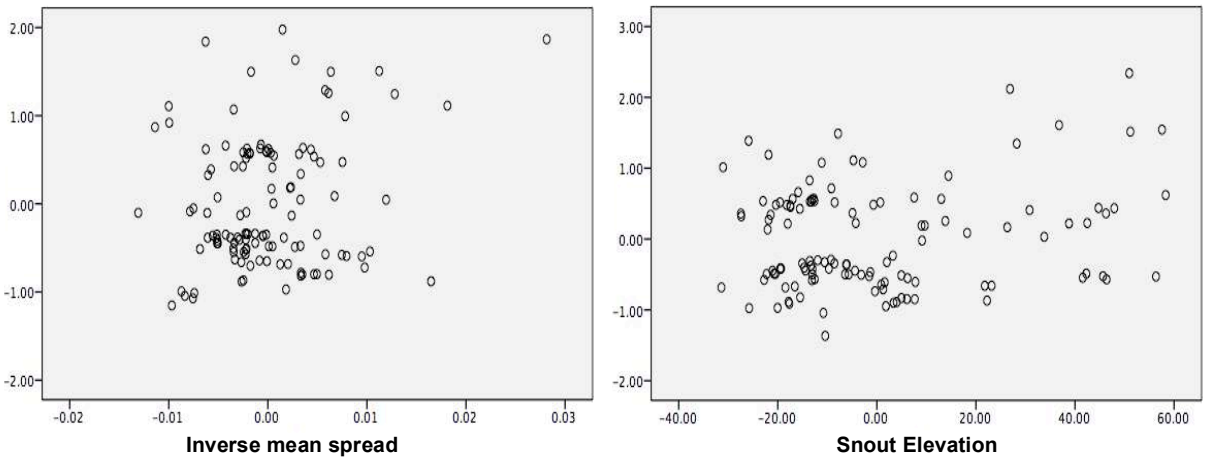

Figure S5. Residual plots showing relationship between inverse mean spread and snout elevation and the number of contacts on tracked whiskers

6 Wall and floor contacts in reconstructed whisker tip trajectories

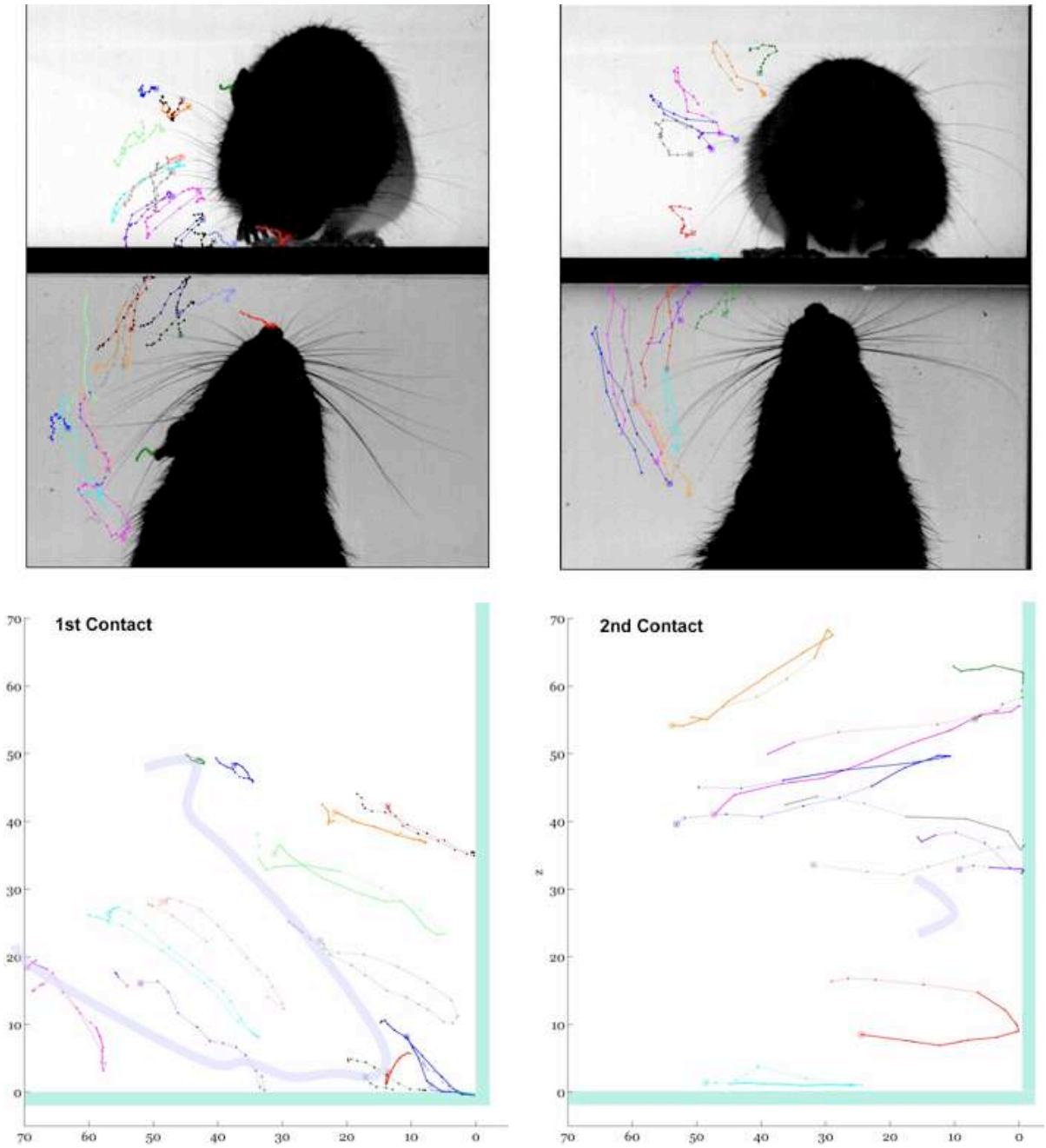

Figure S6. **Whisker tip trajectories for a 1st contact (left) and a 2nd contact whisk (right) plotted in two camera views and in a reconstructed side-on view.** Colored lines show trajectories of individual whiskers matched across views using a least mean square error minimization algorithm. The tip of the snout (red), and of the right ear (green), were tracked in the 1st contact whisk (left) allowing the position of the head to be approximated (purple outline). In the 2nd contact whisk points on the head could not be tracked in both views, hence only the approximate position of the snout is shown. The glass floor and end-wall are also depicted (light blue). Axes show distance to wall and height above the floor in millimeters. The video clips from which the tracks were reconstructed are provided as Supplementary Videos 2 and 3 with whisker matches overlaid.

7 Additional analyses of time from contact to maximum protraction

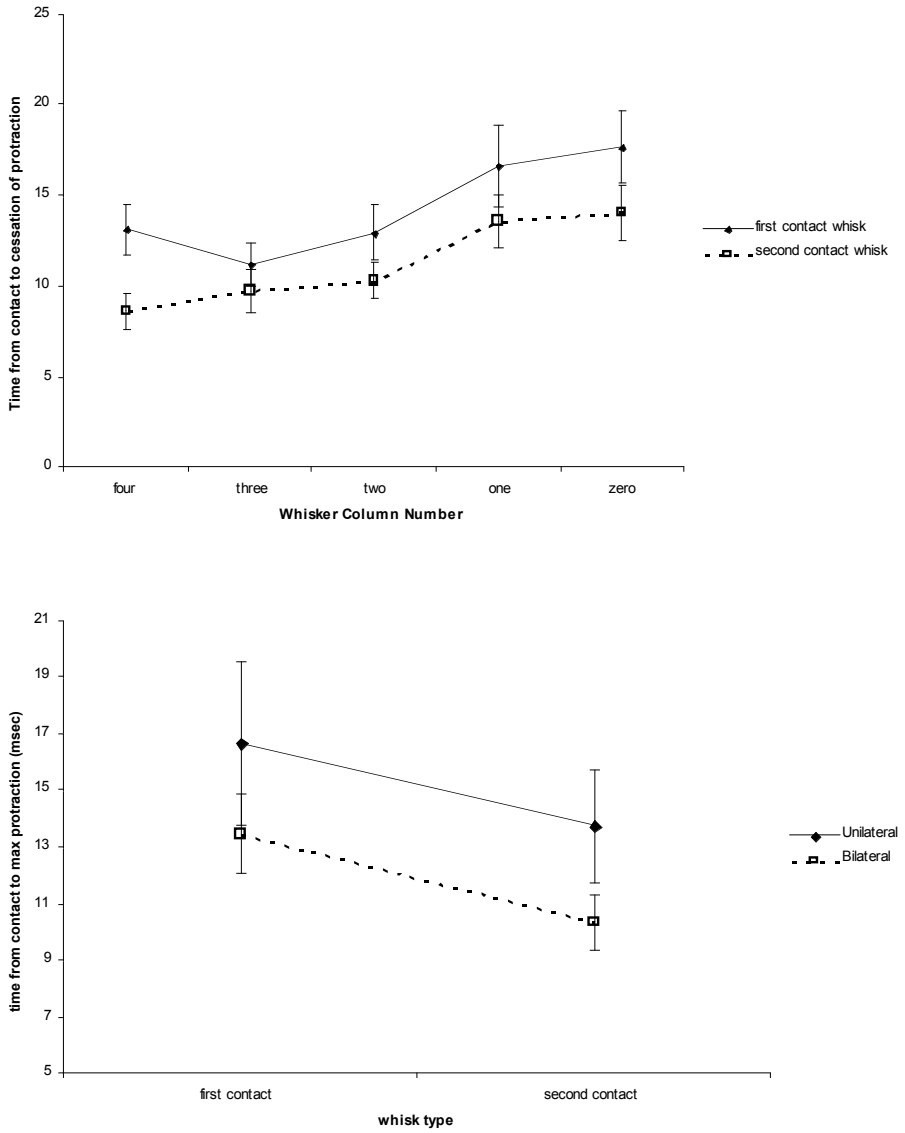

Figure S7. Mean time from contact to maximum protraction in 1st and 2nd contact whisks, analysed per whisker (top) per contact type (bottom). In the analysis by tracked whisker (top) the mean time to maximum protraction was found to be lower in the 2nd contact whisk across all whisker columns, suggesting a consistent effect. Retraction also began upto 5 milliseconds later in the most caudal whiskers. In the analysis of contact type (bottom), cessation of protraction occurred somewhat faster in 2nd contact whisks (compared to 1st contact whisks) and following bilateral contacts (compared to unilateral contacts). A 2x2 ANOVA on this data found no main effect for whisk type ($F_{(1,58)}$ = 3.686, p=0.060) or contact type (bilateral vs. unilateral: $F_{(1,58)}$ = 2.879, p=0.095), and no interaction ($F_{(1,58)}$ = 0.003, p= 0.956), however, it is worth noting that the differences due to whisk type and contact type were approaching significance. Means (s.d.s) for 1st, 2nd contact whisks were unilateral 16.7 (11.6), 13.7 (8.0); bilateral 13.5 (9.3), 10.4 (6.4).

8 Regression analysis for contact duration

Potential predictors for contact duration

Head position and movement	*Pearson's r*	*p*
Distance to wall	-0.051	0.622
Inverse distance to wall	+0.014	0.898
Head orientation	-0.031	0.768
Snout elevation	+0.145*	0.161
Angle of whisker contact with wall	-0.118*	0.256
Velocity towards wall	-0.227*	0.027
Snout vertical velocity	-0.299*	0.003
Whisker control		
Mean protraction velocity	-0.185*	0.073
Mean retraction velocity	-0.129*	0.160
Time from contact to max protraction	+0.466*	<0.001

Correlations calculated for all 1st contact whisks and 35 2nd contact whisks (n= 95)
**= selected for inclusion in regression (r>0.1)*

Final model

Adjusted R square= 0.391, $F_{(1,118)} = 16.072$, $p<0.001$ (using the step-wise method)

Predictor variable	*β*	*p*	*Part correlation*
Time from contact to max. protraction	0.498	<0.001	0.487
Mean retraction velocity	-0.298	<0.001	-0.293
Snout vertical velocity	-0.250	0.003	-0.246
Snout elevation	0.187	0.025	0.183

Velocity towards wall, angle of whisker contact, and mean protraction velocity were not significant predictors.

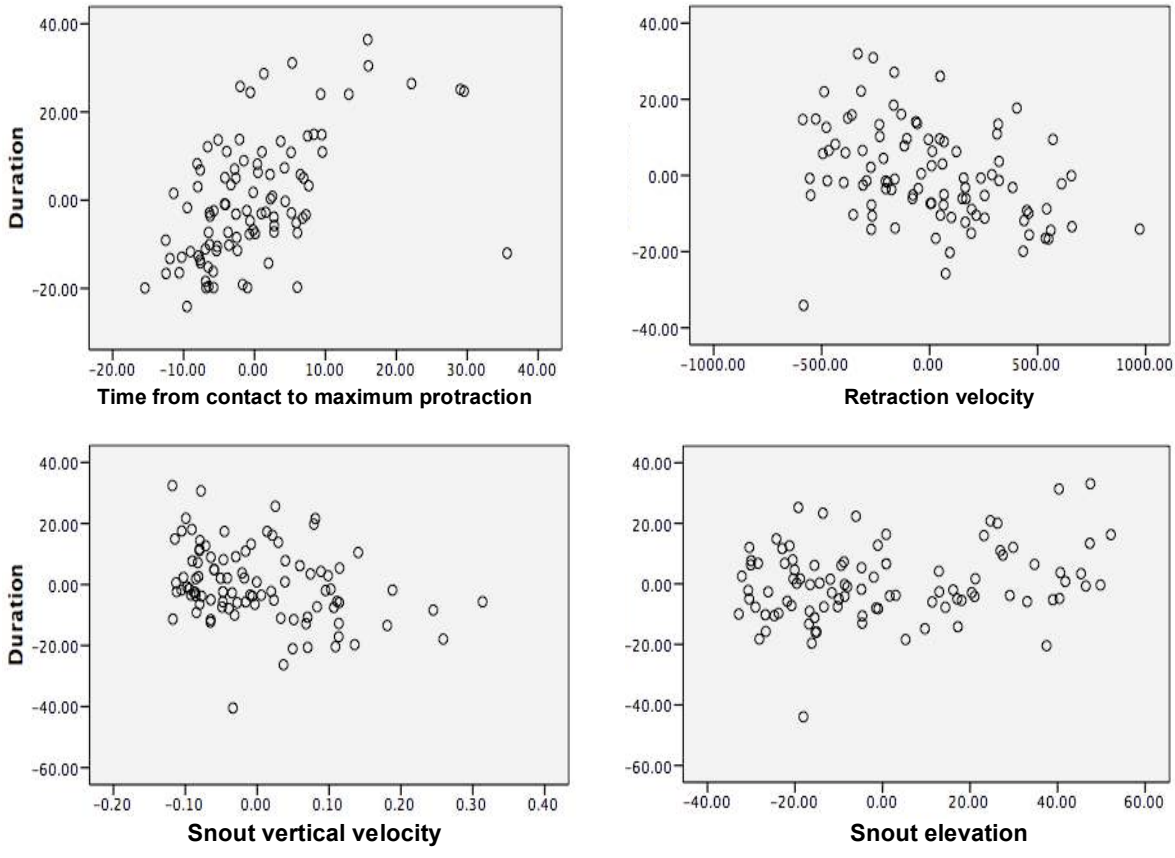

Figure S8. Residual plots showing relationship between time from contact to maximum protraction and retraction velocity and contact duration

9 Retraction velocity and whisk phase

Analyses of retraction velocity for 1st (h1) and 2nd (h2) halves of the retraction phase and for the most rostral (col. 4) and most caudal (col. 0) tracked whiskers

Measure	Mean, standard dev.			% change		ANOVA			
	Pre-contact	1st Contact	2nd Contact	1st	2nd	$F_{(2,118)}$	p	Partial η^2	Post-hoc
Overall mean (Table 2)	*0.89, 0.32*	*0.92, 0.32*	*0.70, 0.35*	*+2%*	*-22%*	*11.33*	*<0.001[a]*	*0.161[d]*	*p,1>2*
H1 mean	1.05, 0.48	0.92, 0.48	0.48, 0.35	-12%	-54%	46.013	<0.001[a]	0.438 [d]	P,1>2
H2 mean	0.86, 0.43	0.92, 0.41	0.78, 0.48	+7%	-9%	1.458	0.237	0.024	n.a.
Col. 4 h1 (rostral)	1.171, 0.643	1.086, 0.592,	0.622, 0.466	+6%	-47%	25.173	<0.001[a]	0.303 [d]	P,1>2
Col. 0 h1 (caudal)	0.646, 0.453	0.448, 0.389	0.329, 0.333	-30%	-49%	10.764	<0.001[a]	0.157 [d]	P>1,2

a. significant using Bonferroni corrected alpha of 0.0125
b. incorporates Greenhouse-Geiser correction for non-sphericity
c. medium-size effect ($0.06 < \text{partial } \eta^2 \leq 0.14$)
d. strong effect (partial $\eta^2 > 0.14$)

For post-hoc tests p= pre-contact, 1= 1st contact, 2= 2nd contact, n.a.= not applicable